Micro- and Nanospectroscopy and Detector Characterization in the IR and THz Range at the Metrology Light Source

Peter Hermann*, Arne Hoehl, Andrea Hornemann, Bernd Kästner, Ralph Müller, Burkhard Beckhoff, Gerhard Ulm

* Peter Hermann, Working Group "IR spectrometry", e-mail: peter.hermann@ptb.de

Introduction

Electron storage rings as synchrotron radiation sources had first been used for the generation of highly brilliant radiation from the vacuum UV to the X-ray spectral range. Due to this high brilliance (or spectral radiance) – which even in the infrared (IR) range is higher by two to three orders of magnitude than that of thermal sources – and the broadband of the synchrotron radiation spectrum, storage rings have, since the beginning of the 1980s, also been used as IR radiation sources [1]. In addition to the high brilliance, the high degree of polarization and the time structure of the synchrotron radiation (SR) with pulse durations in the ps range are also of advantage in the IR range. Today, SR in the IR range is being used at approximately 30 storage rings worldwide [2]. Based on the high brilliance, particularly microspectroscopy with a spatial resolution up to the diffraction limit is performed in the mid infrared (MIR) and in the far infrared (FIR). Many of the applications lie in the field of material sciences, biology or medicine [2–4].

In the course of more than 30 years, PTB has gained experience in the use of SR for metrology at the storage rings BESSY I and II (not, however, in the IR range) [5, 6]. The IR range has been made accessible to PTB only at the *Metrology Light Source* (MLS), where two dedicated beamlines have been installed for the IR and the terahertz (THz) range [6, 7]. Already in the planning phase, the MLS itself has – as the first storage ring worldwide – been optimized to generate coherent radiation in the THz range with radiant powers of up to 60 mW in the special operation mode with particularly short stored electron bunches [8–10].

In the following, selected fields of work at these beamlines will be presented.

FTIR microspectroscopy and secondary structure analysis on biomolecules

In Fourier Transformed Infrared (FTIR) Spectroscopy, a measured interferogram is converted into a spectrum by means of Fourier transformation [11]. At the MLS, bioanalytical investigations with a vacuum FTIR spectrometer (BRUKER Vertex80v), among other things, are performed. The spectral resolution of the Vertex80v amounts to 0.07 cm^{-1}. The attached HYPERION 3000 microscope has been optimized for the MIR range and is equipped with a 128^2-Pixel-Focal-Plane-Array detector for spatially resolved spectroscopy. With a 15x-Cassegrain objective, a resolution of approx. 3 µm is achieved. The MIR range is particularly well suited to excite valence and deformation vibrations of the molecule groups contained in proteins [12, 13]. These MIR signatures, which are also called molecular fingerprints, allow a distinct identification of biomolecules. In addition, IR radiation is not ionizing and allows a non-destructive chemical analysis of biological samples.

At the MLS, FTIR-spectroscopic investigations can also be carried out in the FIR and in the THz range. Here, molecular information, such as rotational bands of the carbon skeleton and hydrogen bonds which occur, for example, in biomolecules, become accessible, in addition [14]. Although the bands occurring there are less complex compared to the modes in the MIR range and, in addition, thermally broadened, they, too, provide information about the structure of biomolecules.

In the MIR range, the group frequencies which are characteristic of proteins (e.g. specific amide bands) are of particular interest for the secondary structure analysis of biomolecules. Thereby, a distinction can be made between different structure types: the α-helix, whose best-known representative is the deoxyribonucleic acid (DNA), and the β-sheet or the β-loops. If all forms occur

with approximately the same frequency, or if the protein has no recognizable secondary structures, one speaks of a random-coil structure [15]. The cause of these different secondary structure motifs inside a protein is hydrogen bonds and characteristic bond angles between the peptide bonds via which the amino acid sub-units of the primary structure are interlinked.

The amide-I-band, which results from C=O stretching vibrations of the peptide skeleton inside a protein, is particularly suited for secondary structure analyses [16]. Changes to the external parameters (pH value, temperature) and interactions with other biomolecules thus allow investigations of conformational changes[1] that can be detected with high sensitivity with the help of IR spectroscopy [17, 18]. As an example, Figure 1 (a) shows the measured IR signature of a protein – in this case of the bovine serum albumin (BSA) – which exhibits α-helical secondary structure elements. Characteristic of this secondary structure motif is the amide-I-band at 1654 cm^{-1}.

For the structure analysis, different mathematical procedures such as, for example, 2D correlation analysis, are used [19]. This analysis serves to simplify complex data sets of a mostly hyperspectral nature, to unfold overlapping bands, and to increase the spectral resolution by plotting the bands against each other over the second dimension. As an example, Figure 1 (b) shows the 2D correlogram Φ^2 associated with the data in Figure 1 (a).

In the 2D correlation plots, so-called autopeaks can be seen along a virtual diagonal which illustrate the spectral range of the highest absorption changes caused by temperature influence on the sample system. In contrast to this, values close to zero indicate a low spectral temperature dependence. Peaks outside the diagonal represent simultaneous changes in the absorption which are observed at two different wavenumbers ν_1 and ν_2 and, thus, suggest the same origin of the change.

At the MLS, SR-based FTIR spectroscopy is used for the fundamental structure analysis on peptides within the scope of a project[3] of the European Metrology Research Programme (EMRP) from the MIR up to the THz spectral range. Amino acids, and the peptides based on them, open up new diagnostic possibilities, for example in cancer research. Furthermore, if the properties of the active substances of peptides, which are based on molecular interaction mechanisms, are exactly known, drugs can be developed which allow illnesses to be treated more effectively. The project deals with the investigation of secondary structure motifs of model peptides which may exert different interaction mechanisms with artificial membrane systems (here: liposomes). It is the main objective of this research project to introduce all results obtained from diverse bioanalytical methods for molecular-dynamic simulations in order to validate the properties of the active substances of peptides.

Another EMRP project is aimed at characterizing biomedical products (stent systems, implants) under process-analytical aspects. The determination of the elementary composition of implant materials as well as the detection of surface contaminations are further aspects of the project. In addition, a method validation based on investigations on model systems and on real-material systems is being aimed at.

Infrared near-field microscopy and nano-FTIR-spectroscopy

The achievable spatial resolution of conventional optical methods is limited by diffraction so that structures smaller than half the wavelength of the incident light can no longer be resolved. In the case of near-field microscopy, the resolution limit given by the wave nature of light is avoided by also using the so-called evanescent waves – and not only the propagating waves – close to the sample surface. These waves also contain information about surface structures which may be clearly smaller than the wavelength of the incident radiation. This makes optical investigations with a spatial resolution at the nanoscale possible.

Scattering-near-field optical microscopes [20, 21] are mostly based on the functional principle of scanning force microscopy, by which spatially resolved optical information is

1 This relates to the change in the spatial structure of a protein.

2 The amplitude Φ is calculated via

$$\Phi(\upsilon_1,\upsilon_2)=\frac{1}{m-1}\Sigma_{j=1}^{m}A_j(\upsilon_1)A_j(\upsilon_2)\ ,$$

with $A_j(\nu_k)$ being the spectral absorption related to the absorption averaged over the temperature, for m spectra in a specific temperature interval.

3 http://projects.npl.co.uk/HLT10-BiOrigin/ (retrieved: 2015-07-07)

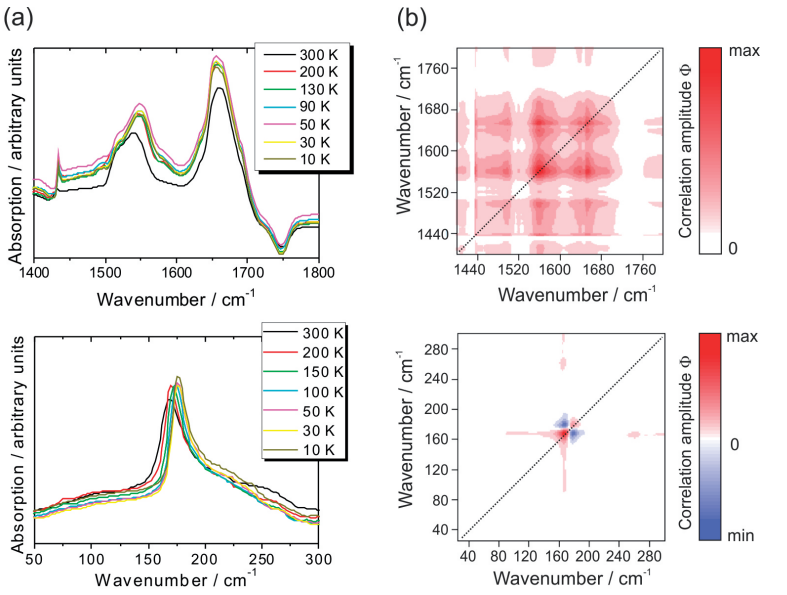

Figure 1:
(a) Signatures of BSA in the MIR (top) and FIR (bottom). (b) 2D correlation diagrams $\Phi(\nu_1,\nu_2)$, showing the temperature dependence of the bands in the amide I (top) and amide VII ranges (bottom).

gained due to the interaction of the probe with the electromagnetic near field of the sample. For this purpose, a near-field probe is brought into a focused light beam, and the light scattered on it is detected. The achievable spatial resolution is determined mainly by the tip radius of the near-field probe used which is typically below 50 nm and, thus, clearly below the optical diffraction limit. In addition to the spatial resolution, the detection sensitivity can be increased so that both weakly absorbing materials and samples with a tiny scattering volume can still be investigated [21]. By lateral probing of the sample one now obtains – in addition to the topographic image – also information about the optical properties of the surface with precisely this improved spatial resolution in the nanometer range.

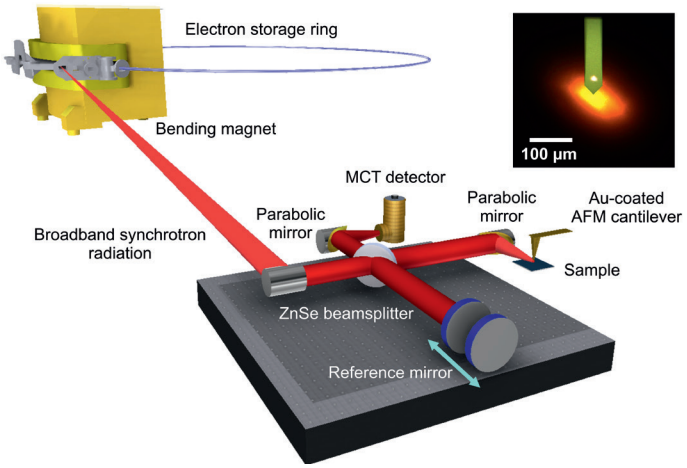

Figure 2:
Schematic representation of the scattered light near-field microscope at the MLS using broadband SR of a bending magnet of the MLS. The radiation is directed via several mirrors (not shown here) to the near-field microscope and focused onto the AFM cantilever. The focused IR beam has a diameter of approx. 80 µm (see microscope image top right). The signal scattered on the tip is detected by an IR-sensitive detector (MCT = *mercury cadmium telluride*).

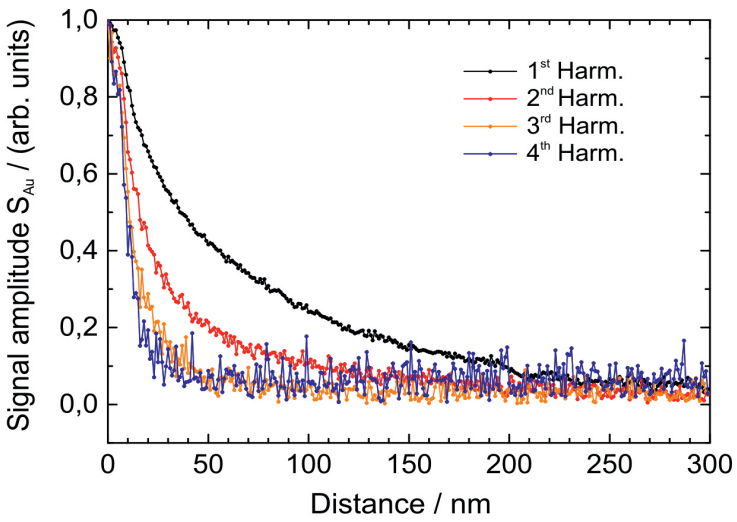

Figure 3:
Decrease in the signal amplitude as a function of the distance between the tip and the sample surface. The scattered signal is demodulated at the higher harmonics of the oscillation frequency of the cantilever to separate the intensive far-field signal from the weak near-field contribution. In the case of a high near-field fraction, the signal decays within less than 50 nm.

As a rule, monochromatic IR light sources – in most cases lasers (e.g. tunable CO or CO_2 gas lasers) – are used for near-field microscopy in order to image the optical properties of a sample surface at a fixed wavelength. In most cases, commercially available Au- or Pt-coated Si cantilevers are used as near-field probes which are excited to oscillations in the frequency range of a few hundred kHz vertically to the sample surface. To separate the intensive far-field signal from the relatively weak near-field contribution, the near-field signal is detected by demodulation of the signal in the higher harmonics of the cantilever's oscillation frequency. Thereby, the strongly exponential decay of the near-field signal, compared to the comparatively constant far-field signal, is exploited.

In 2012, PTB started to establish, in cooperation with the *Freie Universität Berlin* (Working Group of Prof. E. Rühl), a commercially available scattering-type scanning near-field optical microscope at the IR beamline of the MLS (Figure 2). The fundamental aim was to utilize the high brilliance and the defined polarization of the broadband IR SR for performing nano-FTIR spectroscopy in an extended spectral range.

As early as in September 2012 it could be clearly demonstrated worldwide for the first time that a spatial resolution below 100 nm can also be achieved with broadband SR and that nano-FTIR spectroscopy is possible. Figure 3 shows the exponential decrease in the signal amplitude at the higher harmonics of the cantilever's oscillation frequency which is typical of the near-field signal detection. Whereas in the case of the 1st harmonic, the signal decays to the noise level only at a distance of about 200 nm between the tip and the sample surface, the signal amplitude of the 2nd, 3rd and 4th harmonic strongly decreases already after approx. 50 nm.

As a first step towards nano-FTIR spectroscopy, several near-field scans were carried out on an Au layer or across an Au/SiC edge (as summarized in Figure 4). Slight contaminations on the Au surface (diameter: less than 100 nm) can be clearly seen in both the topography image and in the simultaneously recorded optical image. During the scanning across the Au/SiC edge, the optical signal changes within less than 100 nm [22]. By a further optimization of the set-up, a spatial resolution of less than 40 nm has meanwhile been achieved [23].

In a second step, the device was equipped with the Michelson interferometer shown in Figure 2 for the recording of near-field spectra. The reference arm contains a movable mirror to detect the intensity change as a function of the optical path

length difference. The second arm of the interferometer contains the near-field probe and the sample. In the resulting nano-FTIR-spectrum – recorded, for example, of a SiC surface – the characteristic phonon resonance appears at approx. 920 cm^{-1} (Figure 5). As this pronounced phonon resonance can be seen only in near-field spectra, the observation is regarded as a clear demonstration of successful nano-FTIR- spectroscopy. Figure 5 shows the interferograms (5a) and the corresponding nano-FTIR spectra (5b) recorded from differently thin layers [23].

In principle, the use of broadband SR allows the characterization of thin layers and nanostructures in a broad wavenumber range from 700 cm^{-1} to 3400 cm^{-1} by near-field spectroscopy. Possible applications of near-field microscopy and nano-FTIR-spectroscopy are currently investigated within the scope of EMRP projects. For example, within the scope of the EMRP Nanostrain project, SR-based nano-FTIR spectroscopy is evaluated for the characterization of the intrinsic strain in semiconductor and piezoelectric nanostructures[4].

Characterization of radiation detectors by ultra-short pulses of coherent synchrotron radiation

In a special operation mode, the MLS can be used to generate coherent SR (CSR) in the range of THz radiation, whereby the pulse lengths of the radiation pulses lie in the range from 10 ps to the sub-picosecond range. In the case of this special operation mode, the THz spectrum covers a useful wavenumber range from 1.4 cm^{-1} to 50 cm^{-1} (corresponding to a wavelength of 7 mm to 200 µm). The ratio of the intensities from coherent to incoherent SR amounts to 10^5 at maximum, while the stability amounts to up to 0.3 % [7]. The CSR can be optimally used on the dedicated THz beamline which has been designed for the wavelength range from 100 µm to 7 mm.

CSR is used in the following projects: Transmission spectroscopy of peptide films on an FTIR spectrometer, lifetime measurement of excitations of different dopant atoms on a THz pump-probe arrangement of the *Deutsches Zentrum für Luft- und Raumfahrt* (DLR, German Aerospace Center) [24], as well as characterization of the spectral sensitivity and temporal resolution of radiation detectors on a detector testing set-up. The latter allows us to perform investigations such as linearity measurements, determination of the polarization dependence as well as measurements of the time-dependent response of novel THz detectors [25]. As possible detectors for the time-dependent characterization of CSR-THz pulses, superconducting bolometers or Schottky diodes come into consideration. With an YBCO-based bolometer, CSR-THz pulses with a temporal resolution of better than 20 ps could be demonstrated on this set-up [25]. YBCO detectors have, however, the disadvantage that they must

4 http://www.piezo-institute.com/resources/emrp-nanostrain/ (retrieved: 2015-07-07)

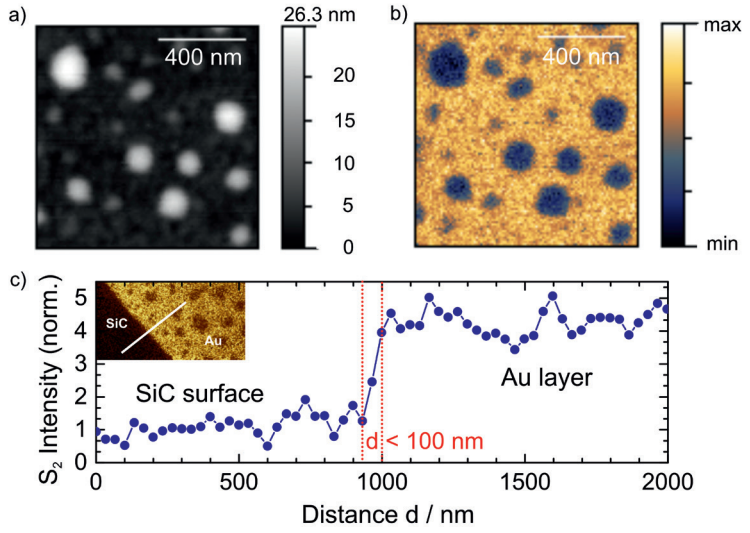

Figure 4:
Topography (a) and simultaneously recorded optical image (b) of an Au surface. Due to the different optical properties, the contaminations appear on the Au surface as dark areas. A scan performed across a SiC/Au edge shows that a spatial resolution *d* of clearly below 100 nm can be achieved (c).

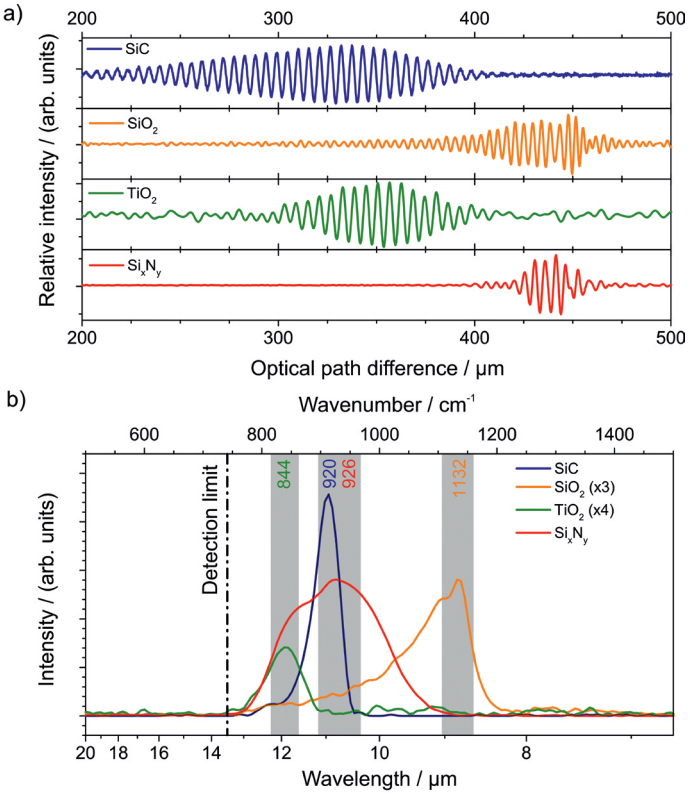

Figure 5:
Interferograms, recorded from different layers: "solid" 6H-SiC, SiO_2 (30 nm in thickness), 10 nm TiO_2 (anatase) and 50 nm Si_xN_y. The associated nano-FTIR- spectra are obtained by subsequent Fourier transformation (b). For better comparability, the spectra of SiO_2 and TiO_2 have been scaled. The numbers in the color of the respective curve indicate the wavenumbers (in cm^{-1}) of the respective peak intensities [23].

be cooled with liquid nitrogen and are, therefore, usually installed in a larger dewar. Here, Schottky diodes offer a possible alternative, as they work under room temperature conditions and are characterized by a compact design [26]. Within the scope of a ZIM project[5] for the *development of an ultra-broadband compact detector for the characterization of THz synchrotron radiation*, these Schottky detectors are currently being investigated. The objective is to improve the response time and to increase the spectral bandwidth. The Schottky diode detector is intended to combine the advantages of planar diode technology with the broadband coupling efficiency of planar antennas. This allows the dimensions of the interface surface between the diode and the antenna to be reduced and, thus, the upper frequency limit of the detection band to be extended. It is expected that these detectors will cover a frequency range from 0.01 THz to 5 THz and have a response time of less than 25 ps [26]. In addition to the THz storage ring diagnostics, further possible applications lie in the field of ultrafast spectroscopy.

5 ZIM (*Zentrales Innovationsprogramm Mittelstand*) is a promotion program of the Federal Ministry of Economics and Energy for SMEs.

References

[1] *G. P. Williams*: Nucl. Instruments Methods Phys. Res. **195**, 383 (1982)

[2] *M. C. Martin, U. Schade, P. Lerch, P. Dumas*: Trends Anal. Chem. **29**, 453 (2010)

[3] *M. C. Martin, P. Dumas*: Spectrosc. Prop. Inorg. Organomet. Compd. **43**, 141 (2012)

[4] *P. Dumas, L. M. Miller, M. J. Tobin*: Acta Phys. Pol. A **115**, 446 (2009)

[5] *B. Beckhoff, A. Gottwald, R. Klein, M. Krumrey, R. Müller, M. Richter, F. Scholze, R. Thornagel, G. Ulm*: Phys. Status Solidi B **246**, 1415 (2009)

[6] *M. Richter, G. Ulm*: in this publication on p. 3

[7] *R. Müller, A. Hoehl, A. Matschulat, A. Serdyukov, G. Ulm, J. Feikes, M. Ries, G. Wüstefeld*: J. Phys. Conf. Ser. **359**, 012004 (2012)

[8] *R. Müller, A. Hoehl, R. Klein, A. Serdyukov, G. Ulm, J. Feikes, M. von Hartrott, G. Wüstefeld*: PTB-Mitteilungen **120**, 229 (2010)

[9] *R. Müller, A. Hoehl, A. Serdyukov, G. Ulm, J. Feikes, M. Ries, G. Wüstefeld*: J. Infrared Milli. Terahz. Waves **32**, 742 (2011)

[10] *J. Feikes, M. von Hartrott, M. Ries, P. Schmid, G. Wüstefeld, A. Hoehl, R. Klein, R. Müller, G. Ulm*: Phys. Rev. ST Accel. Beams **14**, 030705 (2011)

[11] *P. R. Griffiths, J. A. de Haseth*: Fourier Transform Infrared Spectrometry, Wiley, New York (2007)

[12] *E. B. Wilson, J. C. Decius, P. C. Cross*: Molecular Vibrations: The Theory of Infrared and Raman Vibrational Spectra, vol. 102, Dover Publications, New York (1955)

[13] *N. B. Colthup, L. H. Daly, S. E. Wiberley*: Introduction to Infrared and Raman Spectroscopy, Academic Press, New York (1990)

[14] *Y. Marechal*: J. Mol. Struct. **880**, 38 (2008)

[15] *M. Levitt*: Biochemistry **17**, 4277 (1978)

[16] *H. Fabian, C. Schultz, J. Backmann, U. Hahn, W. Saenger, H. M. Mantsch, D. Naumann*: Biochemistry **33**, 10725 (1994)

[17] *K. Kato, T. Matsui, S. Tanaka*: Appl. Spectrosc. **41**, 861 (1987)

[18] *B. Yuan, K. Murayama, Y. Wu, R. Tsenkova, X. Dou, S. Era, Y. Ozaki*: Appl. Spectrosc. **57**, 1223 (2003)

[19] *I. Noda and Y. Ozaki*: Two-dimensional Correlation Spectroscopy – Application in Vibrational and Optical Spectroscopy, John Wiley & Sons, Chichester, West Sussex (2004)

[20] *A. Zayats, D. Richards* (*Eds.*): Nano-Optics and Near-Field Optical Microscopy. Artech House, Boston (2008)

[21] *L. Novotny, B. Hecht*: Principles of Nano-Optics, Cambridge University Press, Cambridge (2006)

[22] *P. Hermann, A. Hoehl, P. Patoka, F. Huth, E. Rühl, G. Ulm*: Opt. Express **21**, 2913 (2013)

[23] *P. Hermann, A. Hoehl, G. Ulrich, C. Fleischmann, A. Hermelink, B. Kästner, P. Patoka, A. Hornemann, B. Beckhoff, E. Rühl, G. Ulm*: Opt. Express **22**, 17948 (2014)

[24] *A. Pohl, A. Hoehl, R. Müller, G. Ulm, M. Ries, G. Wüstefeld, S. G. Pavlov, H.-W. Hübers*: Terahertz pump-probe experiment at the synchrotron light source MLS, Extended Abstracts of IRMMW-THz 2013, TU5-4, Mainz, 1–6 (2013)

[25] *P. Probst, A. Scheuring, M. Hofherr, D. Rall, S. Wünsch, K. Il'in, M. Siegel, A. Semenov, A. Pohl, H.-W. Hübers, V. Judin, A.-S. Müller, A. Hoehl, R. Müller, G. Ulm*: Appl. Phys. Lett. **98**, 043504 (2011)

[26] *N. Sobornytskyy, A. Lisauskas, C. Weickhmann, R. Jakobi, A. Semenov, H. Hübers, R. Müller, A. Hoehl, O. Cojocari*: Quasi optical Schottky diode detectors for fast ultra-wideband detection, Extended Abstracts of IRMMW-THz 2013, TU8-5, Mainz, 1–6 (2013)